Backbending in ^{50}Cr

G. Martínez-Pinedo,[1] A. Poves,[1] L. M. Robledo,[1] E. Caurier,[2] F. Nowacki,[2] J. Retamosa,[2] and A. Zuker[1,2]
[1]*Departamento de Física Teórica C-XI. Universidad Autónoma de Madrid, E-28049 Madrid, Spain*
[2]*Physique Théorique. Bât.40/1, CRN F-67037 Strasbourg Cedex-2, France*
(Received 30 May 1996)

The collective yrast band and the high spin states of the nucleus ^{50}Cr are studied using the spherical shell model and the cranked Hartree-Fock-Bogoliubov method. The two descriptions lead to nearly the same values for the relevant observables. A first backbending is predicted at $I=10\hbar$ corresponding to a collective to noncollective transition. At $J=16\hbar$ a second backbending occurs, associated to a configuration change that can also be interpreted as a spherical to triaxial transition. [S0556-2813(96)50611-4]

PACS number(s): 21.10.Re, 21.10.Ky, 21.60.Jz, 27.40.+z

In a recent paper [1] we have shown that large-scale shell-model (SM) calculations with the realistic interaction KB3 predict the same intrinsic state as cranked Hartree-Fock-Bogoliubov mean-field calculations (HFB) with the Gogny force for the ground-state rotational band of ^{48}Cr. Thus, we have two complementary views of the problem. The SM wave functions have the proper quantum numbers (angular momentum and particle number) and include correlations needed for a detailed account of the observables, while the mean-field results provide us with a simpler understanding of the intrinsic state on which the rotational ground-state band is built.

In a recent experiment [2], it was found that the agreement with the exact yrast energies is even better than indicated in [1], and new measures are coming [3,4] both in ^{48}Cr and ^{50}Cr that make it particularly interesting to extend to the latter the calculations done in the former. What was already known experimentally [5] indicated some rotorlike behavior in ^{50}Cr at low spin with a probable backbend at $J=10\hbar$. The calculations will show that there is indeed a backbend there, and predict a second one at $J=16\hbar$.

Computational procedures. We start with a reminder of the computational procedures used in [1], which we follow here. In the spherical shell model ^{50}Cr is described in a $0\hbar\omega$ space, i.e., ten particles are allowed to occupy all the states available in the pf shell (m-scheme dimensions $\sim 10^7$). The effective interaction is a minimally modified version of the Kuo-Brown G matrix [6] denoted KB3 in [7]. The single particle energies are taken from the ^{41}Ca experimental spectrum. The effect of core polarization on the quadrupole properties is taken into account by the use of effective charges $q_\pi=1.5$, $q_\nu=0.5$. The secular problem is solved using the code ANTOINE [8], a very fast and efficient implementation of the Lanczos method.

In the intrinsic frame calculations we have used the self-consistent cranking Hartree-Fock-Bogoliubov method with the density-dependent Gogny force [9], adopting the DS1 parameter set [10], which has proven capable of describing successfully many phenomena, and in particular high-spin behavior [11]. The mean-field intrinsic states $|\phi_\omega\rangle$ have been expanded in a triaxial harmonic oscillator basis $|n_x n_y n_z\rangle$ with different oscillator lengths. Ten oscillator shells are included in this calculation in order to ensure the convergence of the mean field results.

The yrast band. In Fig. 1 the SM, HFB, and experimental γ-ray energies $E_\gamma(J)=E(J)-E(J-2)$ are plotted as a function of the angular momentum J for the yrast band. The SM results are very close to the present experimental data. In addition, there is preliminary evidence from the Chalk River McMaster Collaboration [3] and from Legnaro [4] confirming the backbending behavior.

The CHFB results follow the trend of the SM ones but are shifted downwards in energy indicating a much bigger static moment of inertia than in the SM and the experiment. In [1] it was argued that this behavior is the result of a deficient treatment of pairing correlations by the HFB method in the weak pairing regime, but it was shown that this shortcoming does not substantially affect the nature of the intrinsic state.

In both theoretical calculations a second backbending is predicted to take place at $J=16\hbar$. The two backbendings define three regions that will be analyzed below in terms of the changes observed in the occupancies of the relevant spherical orbits and of the evolution of the quadrupole moments.

In Fig. 2 we have plotted the fractional occupancies [$\nu(n,l,j)$ in [1]] of the spherical orbits in the HFB solution (upper panel) and in the SM one (middle panel). The shell contributions to $\langle J_x\rangle$ ($j_x(n,l,j)$ in [1] only make sense in the HFB calculation, and are plotted for the relevant spherical orbits in the lower panel. There are striking similarities between the SM and HFB occupancies, with the HFB results being slightly smoother than the SM ones. Before we exam-

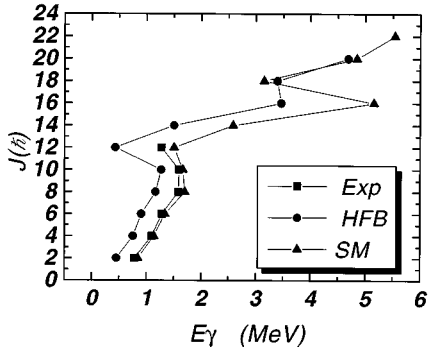

FIG. 1. Theoretical (triangles, SM; circles HFB) and experimental (squares) γ-ray energies versus the angular momentum J.

 © 1996 The American Physical Society

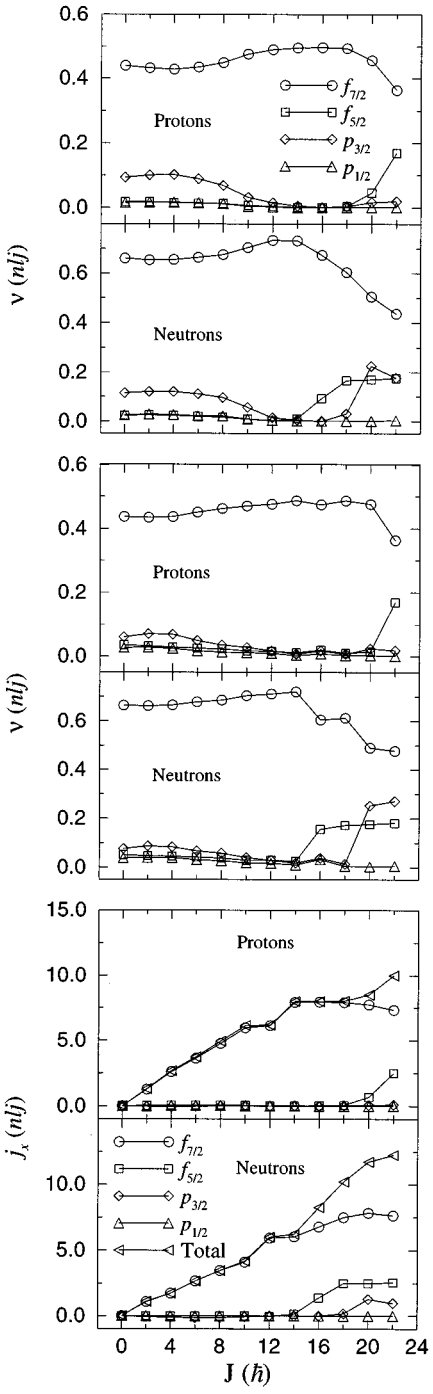

FIG. 2. Upper panel: ''Fractional shell occupancies'' $\nu(n,l,j)$ computed in the HFB approach as a function of J. Middle panel: Same as before but for the SM. Lower panel: ''Shell contribution to $\langle J_x\rangle$'' $j_x(n,l,j)$ in HFB.

ine what these numbers are teaching us in the three regions defined above, it is worth making a brief digression.

Quasi SU3. Although strict Elliott's SU3 symmetry is soon destroyed by the spin-orbit force, it was shown in Ref. [12] that an approximate ''quasi-SU3'' variant—involving the lowest $\Delta j=2$ orbits of a major shell (in our case $f_{7/2}$ and $p_{3/2}$)—can still operate even in the presence of fairly large single-particle splittings. This coupling scheme leads to systematically backbending rotors, and for ^{48}Cr, the schematic calculations in [12] describe quite accurately the features of the results in the full space. When extended to the $(f_{7/2}p_{3/2})^{10}$ space, the same calculations produce rotorlike behavior up to $J=8\hbar$, with large negative Q_s consistent with a constant positive Q_0, and then backbend at $J=10\hbar$, with an abrupt change to positive Q_s that persists for $J=12\hbar$ to $14\hbar$.

It is seen that the yrast states can be described in terms of SM diagonalizations in a small subspace of the full pf shell. The work can be further simplified once it is realized that the eigensolutions depend almost exclusively on the interplay between the single-particle splittings and the quadrupole force. Therefore they must be close to projections of intrinsic states constructed out of Nilsson orbits, and contact with the mean-field methods becomes straightforward. Quasi-SU3 can also provide some extra clues: ^{48}Cr is predicted to be axially symmetric, contrary to its sd shell analogue ^{24}Mg, which is triaxial, as expected from strict SU3. ^{50}Cr, on the other hand, would be triaxial, and the $(f_{7/2}p_{3/2})^{10}$ calculations show indeed a well developed low-lying γ band. Unfortunately it is fragile: as the single particle splittings are increased it moves up in energy and becomes fragmented. As of now, it is difficult to decide whether the experimental and computational efforts necessary to identify possible fragments are worth the trouble but the problem will be examined in a forthcoming paper on $A=47$ and 49 [13].

Returning now to the occupancies, we note in Fig. 2, that up to $J=8\hbar$, next to the dominant $f_{7/2}$ orbit, only its $\Delta j=2$ partner $p_{3/2}$ is appreciably occupied, which, as mentioned in the previous paragraphs, is what we need for rotorlike behavior. Note that the effect is stronger for HFB which, indeed, produces slightly larger $B(E2)$ values as can be gathered in Fig. 3.

The first backbend occurs at $J=10\hbar$, and the calculations differ on the nature of this state: For HFB it still has nonnegligible $p_{3/2}$ occupancy, and hence, quadrupole coherence, while in SM the $f_{7/2}$ dominance is complete, Q_s changes sign and the $B(E2)$ drops abruptly. The discrepancy is minor and amounts to saying that in HFB the $J=10\hbar$ state is transitional, while for SM the change in regime is sudden.

As to what are the states after the backbend, both calculations agree in ^{48}Cr and ^{50}Cr on strong $f_{7/2}$ dominance, and in the lower panel of Fig. 2 we can see that the contribution to the total angular momentum for $J\leqslant 14$ comes fully from the $f_{7/2}$ orbit. At $J=12\hbar$, neutrons have $J=6\hbar$ the maximum attainable by six identical particles. At $J=14\hbar$ both neutrons and protons have reached their maximum value. Therefore, in the region after the backbend we have alignment in the $(f_{7/2})^{10}$ configuration.

To go beyond $J=14\hbar$, the system is forced to promote particles from the $f_{7/2}$ orbit to higher ones and the occupancy plots—which are in nearly perfect agreement for both calculations—show that the promotion takes place first for the $f_{5/2}$ shell. The excitation energy of the 16^+ state is then anomalously large, and leads to the second backbending. At $J=18\hbar$ the $p_{3/2}$ neutron shell reenters the game, leading to the increase in the quadrupole coherence observed in Fig. 3. At $J=22\hbar$ the band terminates as the maximum angular momentum that can be built with four protons and six neutrons in the pf shell is $23\hbar$.

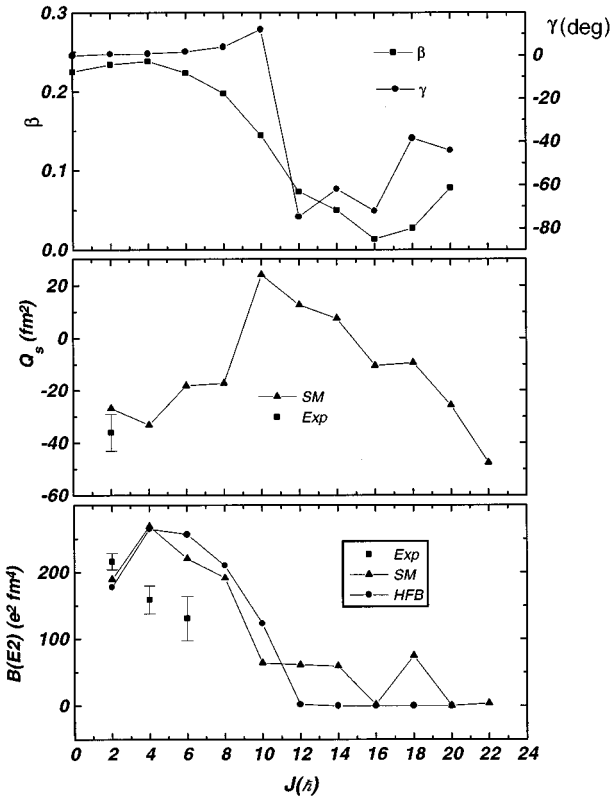

FIG. 3. Upper panel: β and γ deformations in the HFB calculation. Middle panel: Spectroscopic quadrupole moment Q_s computed in the SM approach. The experimental value $Q_s(2^+)$ is also given. Lower panel: $B(E2,\ J\rightarrow J-2)$ transition probabilities versus J computed in SM (triangles) and HFB (circles) compared to the experimental data (squares).

The quadrupole properties obtained in both approaches are summarized in Fig. 3. In the upper panel the β and γ deformation parameters obtained in the HFB calculation [defined as $\beta=\sqrt{(\pi/5)}(Q_{20}^2+Q_{22}^2)^{1/2}/\langle r^2\rangle$ and $\tan\gamma=Q_{22}/Q_{20}$ with $Q_{20}=2z^2-x^2-y^2$ and $Q_{22}=\sqrt{3}(x^2-y^2)$] are plotted versus the angular momentum. We can interpret these results in the three regions as follows.

(i) At low angular momentum ^{50}Cr is an axially symmetric prolate nucleus ($\beta\sim 0.22$ and $\gamma\sim 0$).

(ii) At $J=10\hbar$ the β value drops, and at $J=12\hbar$ the system has clearly become weakly deformed and oblate with $\beta=0.08$ and $\gamma=-67$ degrees. This sudden change corresponds to the observed backbending at $J=10\hbar$.

(iii) At $J=16\hbar$ a second backbending occurs, and the system becomes triaxial.

In the middle panel the spectroscopic quadrupole moments of the SM calculation are plotted as a function of J. In the first region, $J<10$, the values of Q_s [and the $B(E2)$'s, in the bottom panel of Fig. 3] are consistent with a $K=0$ prolate intrinsic state with fairly constant Q_0, corresponding to a value of the deformation $\beta\approx 0.25$, in complete agreement with the HFB picture. Entering the second region, Q_s changes sign abruptly, becoming large and positive for $J=10\hbar,12\hbar$, and $14\hbar$. Simultaneously, the $B(E2)$'s are drastically reduced. These results on the yrast behavior are in line with those obtained by Zamick, Fayache, and Zheng through truncated calculations [14,15].

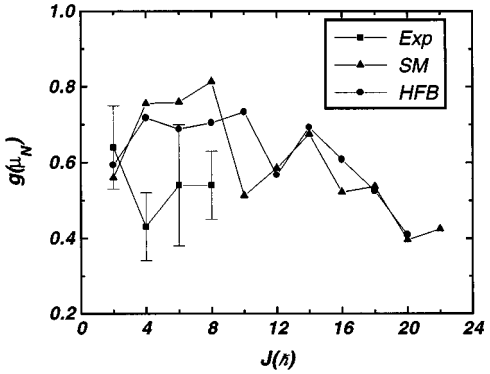

FIG. 4. Gyromagnetic factors: SM (triangles), HFB (circles), and experiment (squares).

The predicted backbends are clearly reminiscent of the ones found in heavier regions, and one would like to relate the present results to the traditional interpretation of backbending in terms of ''band crossing'' (as in Ref. [16]). To obtain some clues we have projected two Nilsson states with $\beta=0.22,\gamma=0$ and $\beta=0.1,\gamma=-60$ (or $\gamma=+60$, both being identical), and then calculated their energies using the full Hamiltonian.

The prolate band reproduces *to the decimal place* the exact Q_s for $J=2\hbar$ and $4\hbar$, but then the agreement deteriorates: ^{50}Cr does not rotate as well as the projected band.

The oblate band hardly describes a rotor, but for $J=10\hbar,12\hbar$, and $14\hbar$ yields (in e fm^2) $Q_s=19.2,11.7,8.3$, respectively, not too far from the exact numbers $(23.7,12.3,7.3)$. Our choice of intrinsic state may not be perfect but it is sufficient to make a crucial point: *the two bands cross between* $J=8\hbar$ *and* $10\hbar$.

Therefore, it seems quite possible to interpret our results for the first backbend in terms of band crossing(s). We have not tried to guess an intrinsic state for the highest spins, but the simple exercise above indicates that the oblate part of the Nilsson diagrams should not be neglected in the search for states of physical interest.

In the lower panel of Fig. 3 the $B(E2)$ transition probabilities from the SM and HFB calculations are plotted as a function of J and compared with the available experimental data. The HFB results are obtained from the intrinsic values of the quadrupole operators Q_{20} and Q_{22} using an improved rotational formula [17]. Both results are very similar in the whole range of angular momentum considered. The comparison with the experiment data is good for the $B(E2,2^+\rightarrow 0^+)$ but both theoretical results overestimate the experimental ones at $J=4\hbar$ and $6\hbar$.

In Fig. 4 we present our predictions for the gyromagnetic factors compared with the experimental results of Pakou *et al.* [18]. Once again the SM and HFB results are nearly identical for the whole band but they do not agree with the data except for the $J=2\hbar$ state. The situation is somehow puzzling. We know that ^{50}Cr is not as good a rotor as ^{48}Cr; its $B(E2)$'s are smaller and the collectivity, as a function of the rotational frequency, vanishes earlier. Our descriptions of ^{50}Cr overshoot the experimental $B(E2)$ values, indicating that we are obtaining a too large quadrupole collectivity. However, for the gyromagnetic factors, the contrary seems to happen. We need to increase the quadrupole

correlations in order to approach the rotational limit reached by the experiment. It is difficult to move simultaneously in both directions. We have tried another version of the KB interaction called KB′ in [19] that has a smaller gap between the $p_{3/2}$ and the $f_{7/2}$ orbits, thus favoring deformation. As expected, while the g values are reduced [$g(2^+)=0.53$, $g(4^+)=0.60$, $g(6^+)=0.62$, $g(8^+)=0.66$] and nearly agree with the experimental results of Ref. [18], the $B(E2)$'s increase a great deal. We find, for instance $B(E2,4^+\rightarrow 2^+)=415\ e^2$ fm^4, compared to the experimental and KB3 values of 159(21) and 264 e^2 fm^4, respectively. It is difficult to imagine mechanisms that could explain simultaneously the experimental g factors and the experimental $B(E2)$'s.

Further discussion of the high spin region. We have already shown that the double backbending in ^{50}Cr is related to the existence of three different zones in the yrast line. In the first of these regions, up to $J=10\hbar$, the decay proceeds by the usual sequence of $\Delta J=2$ enhanced $E2$ transitions. Here we shall study the decay patterns in the other two zones.

In Fig. 5 we have plotted the yrast band as given by the SM calculation, from the first backbending to the maximum J attainable in the $(f_{7/2})^{10}$ configuration. Beyond $J=10\hbar$ the sequence involves $\Delta J=1$ jumps, and the corresponding $M1$ transitions become the dominant branchs due to the reduction of the quadrupole collectivity in this zone: with the exception of $E2$, $14^+\rightarrow 12^+$, the emitted γ's are mostly $M1$. The predictions for the lifetimes and branching ratios given in the figure are calculated using the measured E_γ's. It should be soon possible to compare these numbers with experimental ones from the McMaster Chalk River Collaboration and from Legnaro [3,4].

At higher energies the yrast band continues in $\Delta J=1$ steps, but the $E2$ mode becomes again dominant. If we choose for instance the 18^+ state as entry point, the sequence would be

$$18_1^+ \overset{E2}{\rightarrow} 16_1^+ \overset{E2}{\rightarrow} 14_2^+ \overset{E2}{\rightarrow} 12_1^+ ,$$

while starting at the 17^+ state would yield

$$17_1^+ \overset{E2}{\rightarrow} 15_1^+ \overset{E2}{\rightarrow} 13_2^+ \overset{M1}{\rightarrow} 12_1^+ .$$

Hence, in the third zone we recover the $\Delta J=2,E2$ pattern, but the decay bypasses the yrast 14^+ and 13^+ states.

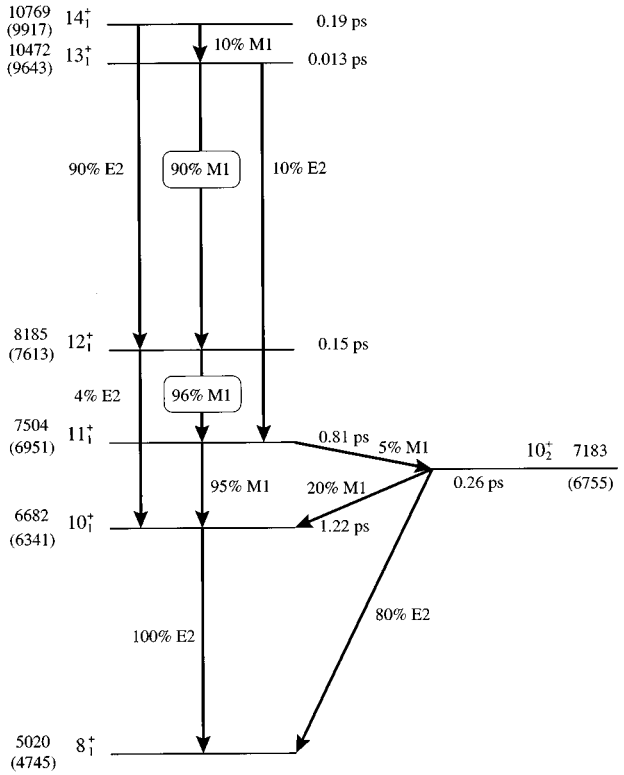

FIG. 5. Decay scheme in the region of the first backbending. Energies in keV. The experimental values are in parentheses.

We have shown that the spherical shell model and the cranked Hartree-Fock-Bogoliubov method give similar descriptions of ^{50}Cr. The structure of the states can be well understood in terms of the schematic quasi-SU3 coupling scheme that provides a natural link between shell model and mean field descriptions.

As far as energetics go, the calculations reproduce accurately the existing observations, and predict a second backbending. For the magnetic and quadrupole properties there is a definite problem in reconciling the different measures. It is to be hoped that ongoing experiments will be of help in clarifying the issue.

We thank Dr. J. A. Cameron and Dr. S. Lenzi for useful discussions. This work has been partially supported by the DGICyT, Spain under Grant Nos. PB93-263 and PB91–0006, and by the IN2P3-(France) CICYT (Spain) agreements. A. Z. is Iberdrola Visiting Professor at the Universidad Autónoma de Madrid.

[1] E. Caurier, J.L. Egido, G. Martínez-Pinedo, A. Poves, J. Retamosa, L.M. Robledo, and A. Zuker, Phys. Rev. Lett. **75**, 2466 (1995).
[2] S.M. Lenzi, D.R. Napoli, A. Gadea, M.A. Cardona, D. Hojman, M.A. Nagarajan, C. Rossi Alvarez, N.H. Medina, G. de Angelis, D. Bazzacco, M.E. Debray, M. De Poli, S. Lunardi, and D. de Acuña, Z. Phys. A **354**, 117 (1996).
[3] J.A. Cameron (private communication).
[4] S. Lenzi (private communication).
[5] T.W. Burrows, Nucl. Data Sheets **75**, 1 (1995).
[6] T.T.S. Kuo and G.E. Brown, Nucl. Phys. **A114**, 241 (1968).
[7] A. Poves and A. Zuker Phys. Rep. **70**, 235 (1981).
[8] E. Caurier, code ANTOINE, Strasbourg, 1989.
[9] D. Gogny, in *Nuclear Self-Consistent Fields*, edited by G. Ripka and M. Porneuf (North-Holland, Amsterdam, 1975).
[10] J.F. Berger, M. Girod, and D. Gogny Nucl. Phys. **A428**, 23c (1984).
[11] J.L. Egido and L.M. Robledo, Phys. Rev. Lett. **70**, 2876

(1993); J.L. Egido, L.M. Robledo, and R.R. Chasman, Phys. Lett. B **322**, 22 (1994); M. Girod, J.P. Delaroche, J.F. Berger, and J. Libert, *ibid.* **325**, 1 (1994).
[12] A. Zuker, J. Retamosa, A. Poves, and E. Caurier, Phys. Rev. C **52**, R1742 (1995).
[13] G. Martínez-Pinedo, A.P. Zuker, A. Poves, and E. Caurier, LANL Report No. nucl-th/9608044, submitted to Phys. Rev. C.
[14] L. Zamick, M. Fayache, and D.C. Zheng, Phys. Rev. C **53**, 188 (1996).
[15] L. Zamick and D.C. Zheng, Phys. Rev. C **54**, 956 (1996).
[16] K. Hara and Y. Sun, Int. J. Mod. Phys. E **4**, 637 (1995).
[17] J.L. Egido and H. Weidenmuller, Phys. Rev. C **39**, 2398 (1989).
[18] A.A. Pakou, J. Billowes, A.W. Mounford, and D.D. Werner, Phys. Rev. C **50**, 2608 (1994).
[19] E. Caurier, A.P. Zuker, A. Poves, and G. Martínez-Pinedo, Phys. Rev. C **50**, 225 (1994).